In vivo cross-linking and transmembrane helix dynamics support a non-piston model of signalling within *E. coli* EnvZ

Rahmi Yusuf[a,1], Tuyết Linh Nguyễn[a,1], Annika Heininger[b], Robert J. Lawrence[a], Benjamin A. Hall[c*] and Roger R. Draheim[a,d*]

[a]School of Pharmacy and Biomedical Sciences, University of Portsmouth, Portsmouth, PO1 2DT, England, UK; [b]Institute of Biochemistry, Biocenter, Goethe University Frankfurt, D-60438 Frankfurt, Germany; [c]MRC Cancer Unit, University of Cambridge, Cambridge, CB2 0XZ, England, UK; [d]Institute of Biological and Biomedical Science, University of Portsmouth, Portsmouth, PO1 2DT, England, UK

Running title: Non-piston transmembrane communication by EnvZ

[1]These authors contributed equally

*To whom correspondence should be addressed (B. A. H. or R. R. D.):

MRC Cancer Unit
University of Cambridge
Hutchison / MRC Research Centre
Box 197, Cambridge Medical Campus
Cambridge
CB2 0XZ
United Kingdom
tel: + 44 (0) 1223 763240
fax: + 44 (0) 1223 763241

University of Portsmouth
School of Pharmacy and Biomedical Sciences
St. Michael's Building
White Swan Road
Portsmouth
PO1 2DT
United Kingdom
tel: +44 (0)23 9284 2133
fax: +44 (0)23 9284 3565

Keywords

porin balance / transmembrane communication / coarse-grained molecular dynamics / sulfhydryl-reactivity / transmembrane helix dynamics

55 In gram-negative bacteria, porins span the outer membrane and control the influx of several
56 prominent groups of antibiotics[1,2]. Thus, it should not be surprising that expression of these porins
57 is often altered in clinical isolates that exhibit multidrug resistance (MDR)[3-9]. The major regulator
58 of porin expression in *Escherichia coli* is EnvZ, a canonical sensor histidine kinase (SHK). It
59 allosterically processes periplasmic interactions with MzrA and cytoplasmic osmosensing into a
60 single unified change in the ratio of its kinase and phosphatase activities[10-15]. Unfortunately, the role
61 of the transmembrane domain (TMD) in communicating these signals across the cellular membrane
62 remains not well understood. Here, we employed *in vivo* sulfhydryl-reactivity to probe the
63 dynamics of individual TM2 helices within the TMD and demonstrate that upon stimulus
64 perception, EnvZ employs a non-piston-type mechanism of transmembrane communication. *In*
65 *silico* coarse-grained molecular dynamics (CG-MD) simulations with EnvZ TM2 are in agreement
66 with these *in vivo* results. We conclude by discussing these results within the context of allosteric
67 processing by EnvZ and propose that these results can be used to predict and classify
68 transmembrane communication by various SHKs.
69
70 Most porins involved in antibiotic transport by gram-negative bacteria belong to the classical OmpF
71 and OmpC families[2]. Transcription of these porins is governed by the intracellular concentration of
72 phospho-OmpR (OmpR-P), which is controlled by EnvZ in response to changes in periplasmic
73 interactions with MzrA and environmental osmolarity[10-15] (Figure S1A). At low intracellular levels
74 of OmpR-P, transcription of *ompF* is upregulated, whereas at higher levels of OmpR-P,
75 transcription of *ompF* is repressed and transcription of *ompC* is activated. This results in a
76 predominance of OmpF at low osmolarity and OmpC at higher osmolarities or in the presence of
77 MzrA (Figure S1B)[16-18]. Dramatic modification of porin balance, which has been observed within
78 clinical isolates from patients undergoing antibiotic treatment, strongly suggests that the underlying
79 mechanisms of porin regulation by EnvZ require further characterisation[3-9]. In addition, it was

80 recently shown that mutations in EnvZ within a porin-deficient (*ompC*$^-$ *ompF*$^-$) *E. coli* strain also
81 resulted in increased carbapenem resistance[19]. Thus, EnvZ plays a not well-understood role in
82 mediating antibacterial resistance that warrants further elucidation.
83
84 Comparison of recently published *apo* and *holo* high-resolution (~1.9 Å) crystal structures of the *E.*
85 *coli* nitrate sensor NarQ that contain the periplasmic, TM and HAMP domains reveal extensive
86 structural rearrangements involving a piston-like motion of TM1 relative to TM2 of approximately
87 2.5 Å. These displacements result in a lever-like rotation of individual HAMP domains upon
88 binding of cognate ligand[20]. Based on these results, the authors posit that receptors containing a
89 membrane-adjacent HAMP domain function by a piston-type displacement of TM helices while
90 those that lack such domains transduce signal by rotation of TM helices. We previously postulated a
91 related yet different categorisation of signalling mechanisms also based on the domain structure of
92 bacterial receptors[21]. We proposed that receptors containing a periplasmic four-helix bundle
93 transduce signal across the membrane by piston-type displacements and that the attached
94 membrane-adjacent HAMP domains might possess one of a multitude of signalling mechanisms
95 including a gearbox-type rotation[22], a dynamic bundle[23] or potentially other mechanisms[21].
96 Differentiating between these classification systems will provide a theoretical framework for
97 understanding domain-based intra-protein allosteric communication by bacterial receptors.
98
99 Here, we have analysed transmembrane signalling within EnvZ for several reasons. Firstly, because
100 of its aforementioned importance in regulating bacterial porin expression. Understanding how EnvZ
101 transduces signal would be a significant step toward direct manipulation of porin balance in
102 bacterial cells exhibiting MDR. Secondly, it examines whether SHKs that possess membrane-
103 adjacent HAMP domains function solely by piston-type displacements or whether other signalling
104 mechanisms might be employed. The results here with EnvZ are compared with previous findings

105 from the aspartate chemoreceptor (Tar) and the recent NarQ structures[20,24-26]. These three are ideal
106 candidates for comparison because they all possess a membrane-adjacent HAMP domain, however,
107 while Tar and NarQ possess a periplasmic four-helix bundle, EnvZ possesses a periplasmic
108 PDC/CACHE domain[27,28].
109
110 *Mapping TM2 surfaces important for EnvZ signal output*
111
112 We previously created a Cys-less version of EnvZ from *E. coli* that had its sole Cys residue
113 changed to an Ala residue (C277A). The Cys-less variant is expressed from pRD400, which results
114 in the addition of a seven-residue linker (GGSSAAG) and a C-terminal V5 epitope
115 (GKPIPNPLLGLDST). We previously found that the Cys-less version of EnvZ had similar steady-
116 state signal output and response to environmental osmolarity as the wild-type version of EnvZ
117 making it suitable for comparisons of *in vivo* sulfhydryl-reactivity and signal output analysis. We
118 initially determined that no major rearrangements occur along the TM1-TM1' interface upon
119 stimulus perception[29]. As minimal change was observed along this helical interface in response to
120 osmolarity, we continued by examining the TM2-TM2' interface. We began by determining which
121 residues comprise TM2 by subjecting the full EnvZ sequence to DGpred[30] and TMHMM v2.0[31],
122 which suggested that Leu-160 to Ile-181 and Leu-160 to Ile-179 comprise TM2 respectively. Based
123 on these analyses, we employed site-directed mutagenesis using the Cys-less variant as a template
124 to create a library of single-Cys-containing EnvZ proteins that spanned from positions 156 to 184
125 (Figure 1). We observed that nearly the entire library was expressed within EPB30/pRD400 cells
126 grown under the low- or high-osmolarity regime. Variants possessing a Cys at position 156 showed
127 low levels of expression when grown under the low-osmolarity (0% sucrose) regime. However,
128 when grown under the high-osmolarity regime, no variants showed reduced expression level
129 (Figure S2). These results indicate that the library is suitable for further *in vivo* experimentation.

130

131 We began by expressing each of the single-Cys-containing variants in EPB30/pRD400 cells, which
132 allowed us to measure CFP fluorescence, YFP fluorescence, and to calculate the CFP/YFP ratio that
133 estimates steady-state EnvZ signal output (Figure S1B). Cells expressing the Cys-less C277A were
134 used as a baseline comparison (Figure S3). When EPB30/pRD400 cells are grown under the low-
135 osmolarity regime, a shift in signalling output toward the "on" or kinase-dominant state results in
136 increased CFP fluorescence, reduced YFP fluorescence and an increase in the overall CFP/YFP
137 ratio, while a shift toward the "off" or phosphatase-dominant state appears as decreased CFP,
138 increased YFP and a decrease in CFP/YFP ratio (Figures 2 and S4).

139

140 Several trends were observed during analysis of the library of Cys-containing EnvZ receptors.
141 When EPB30/pRD400 cells were grown under the low-osmolarity regime, EnvZ was less tolerant
142 of Cys substitutions at the N- and C-terminal regions of the library. At the N-terminus, signal output
143 from receptors containing a Cys at positions 156, 162 and 163 were very elevated, exhibiting
144 greater than a 5-fold increase in CFP/YFP, while receptors possessing a Cys in the C-terminus at
145 positions 179, 181, 182 and 184 were elevated, possessing over a 2-fold increase in CFP/YFP.
146 These boundary regions appear to flank a core of alternating increases and decreases in EnvZ signal
147 output, as observed between residue positions 165 and 180, suggesting that multiple tightly packed
148 EnvZ helices exist within the hydrophobic core of the inner membrane (Figures 2A and 2B). When
149 grown under the high-osmolarity regime, a pattern appeared where Cys substitutions resulted in
150 significant decreases in signal output (Figure 2C). Of the 29 mutants analysed, 13 supported less
151 than 75% of the normal wild-type signal output.

152

153 Perhaps most striking is the inverse effect on EnvZ signal output of the Cys substitutions that flank
154 the hydrophobic core of TM2. For these residues, when grown under the low-osmolarity regime, the

155 presence of a Cys residue resulted in an increase in signal output of more than 25%, i.e. shifted
156 toward the on or kinase-dominant state (red dots in Figure 2A) and a reduction in signal output of
157 more than 25%, i.e. shifted toward the off or phosphate-dominant state, when grown under the high-
158 osmolarity regime (blue dots in Figure 2C). These flipped positions reside at the N- and C-terminal
159 ends of the region we examined and outside of the proposed hydrophobic TMD core (Figure 2).
160 Within the hydrophobic core, Cys substitutions show similar changes when cells are grown under
161 the low- and high-osmolality regimes. These results suggest that the flanking regions are not simply
162 rigid structural conduits for signal transduction but may have higher-order roles in signal
163 transduction, such as MzrA interaction or functioning as a control cable at the N- and C-terminal
164 regions respectively[14,15,23,32-34].

165

166 *Identifying surfaces involved in TM2-TM2' interactions*

167

168 Sulfhydryl-reactivity experimentation is well-characterised and has been employed on many soluble
169 and membrane-spanning proteins and higher-order complexes[35]. The *in vivo* nature of this assay
170 facilitated mapping of the TM2-TM2' interface under different osmotic conditions, which is an
171 important first step toward understanding how EnvZ processes allosteric inputs from periplasmic
172 MzrA binding and cytoplasmic osmosensing into a single uniform modulation of bacterial porin
173 balance (Figures 1 and S1). In a similar manner to mapping TM1-TM1' interactions[29], Cys-
174 containing EnvZ variants were expressed in EPB30/pRD400 cells and upon entering the early
175 exponential phase ($OD_{600nm} \approx 0.25$) they were subjected to 250 μM molecular iodine for 10 minutes
176 analysed by non-reducing SDS-PAGE and immunoblotting (Figure S5).

177

178 We observed three distinct regions within TM2. The N-terminal region (region I in Figure 3),
179 comprised of residues 156 to 163, exhibited significant cross-linking under the low-osmolarity

180 regime (0% sucrose) and almost no crosslinking under the high-osmolarity (15% sucrose) regime.
181 The second region (II) consisting of positions 164 to 179, demonstrated altering low and high levels
182 of disulphide-formation consistent the crossing of TM2 and TM2' within the hydrophobic core of
183 the TMD. The final region (III), from residues 180 to 184, shows no crosslinking (Figure 3). It
184 should be noted that this significant difference at the periplasmic end of the TMD between cells
185 grown under the low- and high-osmolarity regime was not observed during similar analyses of
186 TM1[29].
187
188 *Molecular simulations of the wild-type and aromatically tuned variants of EnvZ TM2*
189
190 The piston-type model of transmembrane communication is founded upon the central tenant that the
191 vertical position of TM2 relative to the lipid bilayer changes upon stimulus perception. Previous
192 work with TM2 of Tar demonstrates that repositioning the aromatic residues at the cytoplasmic end
193 of TM2, known as aromatic tuning[36], repositions the helix within a biological membrane[37] and that
194 this repositioning causes an incremental change in signal output[36]. These results served as an
195 experimental framework to optimise SIDEKICK software capable of high-throughput parallelised
196 coarse-grained molecular dynamics (CG-MD) simulations, which demonstrated that aromatic
197 tuning repositioned the TM2 helix *in silico* in a manner consistent with both the *in vivo* results and a
198 piston-type mechanism of transmembrane communication[38].
199
200 Based on these extensive results and the recent suggestion that mechanisms employed by SHKs
201 during TM communication correlate with the presence of a membrane-adjacent HAMP domain, we
202 performed analogous *in silico* experimentation with EnvZ, which possesses a membrane-adjacent
203 HAMP domain but substitutes a periplasmic PDC/CACHE domain for the four-helix bundle present
204 in Tar and NarQ[20,27,28,39]. We previously performed aromatic tuning with TM2 of EnvZ and found

205 that signal output was not correlated with the absolute vertical position of the aromatic residues as
206 was shown for Tar TM2, which suggested that EnvZ does not transduce signal output across the
207 membrane by a piston-type displacement[40].
208
209 To interpret the results of our GC-MD analysis, we categorised the signal output of these
210 aromatically tuned EnvZ variants[40]. For several two-component signalling circuits, including the
211 EnvZ/OmpR, PhoQ/PhoP and CpxA/CpxR circuits, the steady-state output of the signalling circuits
212 has been shown to be independent of the level of SHK present[40-43]. However, in circuits containing
213 the tuned variants of EnvZ, a different relationship between steady-state signal output and receptor
214 level was observed, suggesting that the ratio of kinase to phosphatase activities was different within
215 each receptor and always different than wild-type EnvZ[40]. Based on this analysis, we found that the
216 WLF-1 variant possessed the highest signal output while the WLF-5, WLF-4 and WLF-3 variants
217 possessed only slightly higher activity than wild-type EnvZ, which maintained receptor-
218 concentration dependent robustness unlike the tuned variants. WLF-2 and WLF+1 were found to
219 possess reduced signal output, while WLF+2 possessed the lowest overall signal output. These
220 differences were previously quantified by analysing the slope of the change in CFP/YFP against the
221 amount of receptor present and are visually represented in Figure S6[40]. These classifications are
222 employed during interpretation of the CG-MD results in Figure 4.
223
224 Based on these previous results and the absence of asymmetric TM2 displacement observed within
225 the *in vivo* sulfhydryl-reactivity assay (Figure 3), we assessed whether molecular simulations would
226 lend credibility to a non-piston type of transmembrane communication employed by EnvZ. We
227 began by designing tuned TM2 sequences to subject to GC-MD simulations that matched those
228 previously used during the aromatic tuning experimentation (Figure 4A). Unlike analogous
229 experimentation with TM2 of Tar, no trend in helix displacement was observed (Figure 4B, Table

230 S1). This indicates that the mutations do not in isolation move the helix up and down in the
231 membrane and would appear to rule out a pure piston motion as previously observed in Tar[38].
232
233 An alternative mechanism for signal transduction is to induce a tilt in the helix relative to the
234 bilayer normal. This was originally proposed in Tar on the basis of crystallographic analysis of the
235 receptor domain[44], and led to the proposal of a "swinging piston" where both displacement and tilt
236 contributed to signal transduction. In addition, this would be consistent with a scissor-type model of
237 TM communication proposed to be utilised by PhoQ[45,46], which possesses a periplasmic
238 PDC/CACHE domain[47]. In testing the tuned EnvZ TM2 helices, a change in the extent of tilting
239 was observed during the CG-MD simulations (Figure 4C, Table S2). It was found that a reduction
240 in tilt, to a mean tilt of between 22 and 24 degrees, compared to the wild-type TM2 sequence with a
241 tilt of approximately 26 degrees correlated with a decreased signal output (phosphatase-biased, dark
242 blue). Interestingly, an increase in tilt to more than 29 degrees correlated with extremely biased
243 signal output, *i.e.* highly kinase-dominant (WLF-1, pink) and highly phosphatase-dominant
244 (WLF+2, bright blue). Taken together, these results demonstrate that tilt, rather than vertical
245 displacement, does correlate with altered signal output from EnvZ.
246
247 Finally, a rotational/gearbox model of TMD-HAMP communication has also been proposed for
248 EnvZ[22,48]. Central to this model is that interconversion between the kinase-dominant and
249 phosphatase-dominant signalling states can be accomplished by rotation of the individual HAMP
250 helices in unison by 26 degrees. Within our simulations, we observed some consistency with the
251 gearbox model of HAMP signalling, especially when the WLF-1 helix possessed a mean azimuthal
252 rotation that is 25 degrees different than wild-type EnvZ (pink in Figure 4D). The full-length WLF-
253 1 receptor was determined to the most highly kinase-biased tuned receptor we studied. The TM
254 helix from the most phosphatase-biased receptor (WLF+2) possessed a mean azimuthal rotation of

255 an additional 15 degrees. For the simulations involving other helices, it was not possible to
256 differentiate them into separate classes.
257
258 Here, our *in vivo* analysis demonstrated that only the periplasmic end of EnvZ TM2 undergoes a
259 conformational transition upon stimulus perception suggesting that the asymmetric piston-type
260 displacement employed by Tar is not used by EnvZ. Previously, a linear correlation was observed
261 between the position of the aromatic residue in Tar TM2, the position of the helices *in vitro* and *in*
262 *silico* and the signal output from each Tar receptor[36,37,40,49]. Here, *in silico* analysis of EnvZ TM2
263 demonstrates that such a linear correlation is absent suggesting that EnvZ functions by a non-piston
264 mechanism in which both tilting and azimuthal rotation play a substantial role in modulation of
265 signal output (Figure 4).
266
267 *Correlations between domain composition and mechanisms of signal transduction*
268
269 The authors of the recent NarQ structures posit that the presence or absence of the membrane-
270 adjacent HAMP domain may be the difference between receptors employing piston-type
271 mechanisms of transmembrane communication as compared to other signalling mechanisms[20].
272 However, differences employed during transmembrane communication by the Tar and EnvZ TMDs
273 observed here and previously strongly suggest that Tar and EnvZ possess different mechanisms of
274 TM communication. Our previous work analysed AS1 helices from *E. coli* NarX, *E. coli* Tar, *E.*
275 *coli* EnvZ and Af1503, the HAMP domain resulting in the initial high-resolution structure[22], and
276 found that the Tar and NarX AS1 helices possess similar properties, which AS1 helices from both
277 EnvZ and Af1503 lack. Recent comparisons of the *apo* and ligand-bound structures of the
278 combined periplasmic-TM-HAMP domain from *E. coli* NarQ demonstrate that binding of ligand
279 results in symmetrical displacements of TM1 relative to TM2 of approximately 2.5 Å.[20] These

280 results are similar to Tar, which functions by asymmetrical TM2 displacement also possesses a
281 periplasmic four-helix-bundle[24-26,39]. Thus, we conclude that *E. coli* EnvZ functions by a non-piston
282 mechanism of transmembrane communication that is different than Tar, NarX and NarQ, which
283 communicate across the membrane by piston-type displacements. Furthermore, we propose that the
284 TM signalling mechanisms can be predicted and assigned based upon the domain(s) present in the
285 periplasmic region of a bacterial TM-spanning receptor.
286
287 **Methods**
288
289 *Bacterial strains and plasmids*
290
291 *E. coli* strains DH10B (New England Biolabs) or MC1061[50] were used for DNA manipulations,
292 while strain K-12 MG1655[51] served a non-fluorescent strain that was used to control for light
293 scattering and cellular autofluorescence. *E. coli* strains MDG147 [MG1655 Φ(*ompF*$^+$-*yfp*$^+$)
294 Φ(*ompC*$^+$-*cfp*$^+$)] [52] and EPB30 (MDG147 *envZ::kan*)[43] were employed for analysis of EnvZ signal
295 output. Plasmid pRD400[40] retains the IPTG-based induction of EnvZ from plasmid pEnvZ[53] while
296 adding a seven-residue linker (GGSSAAG)[54] and a C-terminal V5 epitope tag
297 (GKPIPNPLLGLDST)[55]. As the C-terminus of bacterial receptors can be sensitive to the presence
298 of an epitope tag, we previously ensured that the addition of a V5-epitope tag did not alter the
299 signalling properties of EnvZ[40,56]. Plasmid pEB5[41] was employed as an empty control vector.
300
301 *Selection of residues comprising TM2 of EnvZ*
302
303 The primary sequence of EnvZ from *E. coli* K-12 MG1655 was subjected to DGpred using a
304 minimal window of 9 residues and a maximal window of 40 residues[30]. Alternatively, a software

305 package that identifies TM helices with a Markov model (TMHMM v2.0)[31] was also employed.
306 These software packages suggested that Leu-160 to Ile-181 and Leu-160 to Ile-179 comprise TM2
307 respectively. Based on these results and to maximize the probability of including all residues within
308 TM2, we targeted all residues between positions 156 to 184 for the creation of a library of single-
309 Cys-containing EnvZ receptors.
310
311 *Analysis of EnvZ signal output* in vivo
312
313 Bacterial cultures were grown as described previously[57] with minor modification. MDG147 or
314 EPB30 cells were transformed with pRD400 expressing one of the single-Cys-containing EnvZ
315 receptors or pEB5 (empty). Fresh colonies were used to inoculate 2-ml overnight cultures of
316 minimal medium A[58] supplemented with 0.2% glucose. Ampicillin, sucrose and IPTG were added
317 as appropriate. Cells were grown overnight at 37 °C and diluted at least 1:1000 into 7 ml of fresh
318 medium. Upon reaching an $OD_{600nm} \approx 0.3$, chloramphenicol was added to a final concentration of
319 170 μg/ml. Fluorescent analysis was immediately conducted with 2 ml of culture and a Varian Cary
320 Eclipse (Palo Alto, CA). CFP fluorescence was measured using an excitation wavelength of 434 nm
321 and an emission wavelength of 477 nm, while YFP fluorescence was measured using an excitation
322 wavelength of 505 nm and an emission wavelength of 527 nm. These values were corrected for cell
323 density and for light scattering/cellular autofluorescence by subtracting the CFP and YFP
324 fluorescence intensities determined for MG1655/pEB5 cells.
325
326 *Analysis of sulfhydryl-reactivity* in vivo
327
328 Cells were grown as described above with minor chnges. Upon reaching an $OD_{600nm} \sim 0.3$, cells
329 were subjected to between 250 μM molecular iodine for 10 min while incubating at 37 °C. The

330 reaction was terminated with 8 mM N-ethylmaleimide (NEM) and 10 mM EDTA. Cells were
331 harvested by centrifugation and resuspended in standard 6X non-reducing SDS-PAGE buffer
332 supplemented with 12.5 mM NEM. Cell pellets were analysed on 10% SDS/acrylamide gels.
333 Standard buffers and conditions were used for electrophoresis, immunoblotting and detection with
334 enhanced chemiluminescence[59]. Anti-V5 (Invitrogen) was the primary antibody and peroxidase-
335 conjugated anti-mouse IgG (Sigma) was the secondary antibody. Digitized images were acquired
336 with a ChemiDoc MP workstation (Bio-RAD), analysed with ImageJ v1.49[60] and quantified with
337 QtiPlot v0.9.8.10.
338
339 *CG-MD simulations with SIDEKICK*
340
341 As previously described[38], coarse-grained molecular dynamics (CG-MD) simulations were
342 performed using the MARTINI forcefield with an approximately 4:1 mapping of non-H atoms to
343 CG particles. Lennard-Jones interactions between 4 classes of particles: polar (P), charged (Q),
344 mixed polar/apolar (N) and hydrophobic apolar (C) were used to treat interparticle interactions.
345 Within MARTINI, P and C particle types were subdivided to reflect varying degrees of polarity.
346 Short range electrostatic interactions were treated Coulombically, shifted to zero between 0 and 12
347 Å. Lennard-Jones interactions were shifted to zero between 9 and 12 Å. α-helix integrity was
348 maintained via dihedral restraints. Peptide termini were treated as uncharged. Simulations were
349 performed using Gromacs 3[61]. Temperature was coupled using a Berendsen thermostat at 323 K
350 (τ_T=1 ps), and pressure was coupled semi-isotropically (across XY/Z) at 1 bar
351 (compressibility=3×10^{-5} bar^{-1}, τ_P=10 ps). The initial simulation timestep was 20 fs. Initial models
352 of the TM α-helices were generated as ideal, atomistically detailed α-helices using standard
353 backbone angles and side- chain conformers. These were then converted to coarse-grained as

354 described previously[38]. Around 128 DPPC molecules were used in each simulation along with
355 around 3000 CG water particles, giving a final system size of ~65×65×13 Å.
356
357 **Author contributions**
358
359 R. Y., T. L. N, B. A. H. and R. R. D. conceived and designed the experiments. R. Y., T. L. N., A. H.
360 and R. J. L. performed the experiments. R. Y., A. H., T. L. N., R. J. L., B. A. H. and R. R. D.
361 analysed the data. R. Y., T. L. N., B. A. H. and R. R. D. wrote the manuscript. All authors read and
362 approved the final manuscript.
363
364 **Acknowledgments**
365
366 R. Y. was generously supported by the Indonesia Endowment Fund for Education, Ministry of
367 Finance (S-4833/LPDP.3/2015). T. L. N. was supported by a grant from the Erasmus+ programme.
368 R. R. D. was supported with start-up funding from the Faculty of Science and from the Institute of
369 Biological and Biomedical Science (IBBS) at the University of Portsmouth. B. A. H. was supported
370 by The Royal Society (UF130039).
371
372 **Competing interests**
373
374 The authors declare no competing financial interests.
375
376 **Figure legends**
377

378 Figure 1. EnvZ functions as a homodimer with a cytoplasmic N-terminus, the first transmembrane
379 helix (TM1, white), a large periplasmic domain (sensor, white), the second transmembrane helix
380 (TM2, red), a membrane-adjacent HAMP domain (grey) and the cytoplasmic domains responsible
381 for dimerization and histidylphosphortransfer (DHp, black) and catalytic ATPase activity (CA,
382 black). The position of the original Cys-277 residue that was mutated to Ala to produce the Cys-less
383 EnvZ is provided. The residues subjected to Cys substitution and their position in the primary
384 sequence is provided. Signal output from each single-Cys-containing variant is compared to the
385 Cys-less (C277A) variant: less than 50% of Cys-less (light blue), between 50% and 75% of Cys-
386 less (dark blue), between 75% and 125% of Cys-less (grey), between 125% and 200% (dark red)
387 and greater than 200% (light red). Residue positions exhibited flipped signal output are indicated
388 with a plus. The extent of sulphydryl-reactivity is also presented in five categories based on dimer-
389 to-monomer ratio: no dimer present (white), less than 0.05 (light grey), between 0.05 and 0.2
390 (medium grey), between 0.2 and 0.5 (dark grey) and greater than 0.5 (red). Positions that exhibit a
391 significant change in cross-linking between the low- and high-osmolarity regimes are indicated with
392 a plus.
393
394 Figure 2. Signal output from the library of single-Cys EnvZ variants. (A) CFP/YFP from
395 EPB30/pRD400 cells expressing one of single-Cys variants grown under the low-osmolarity (0%
396 sucrose) regime. On the right axis, these CFP/YFP ratios are compared to the Cys-less (C277A)
397 variant. (B) Magnified version of panel A in order to emphasise the region up to a 2-fold increase in
398 CFP/YFP. (C) CFP/YFP from EPB30/pRD400 cells expressing one of the single-Cys variants
399 grown under the high-osmolarity (15% sucrose) regime. On the right axis, these CFP/YFP ratios are
400 compared to the Cys-less (C277A) variant. The flipped mutants are highlighted with a red dot in
401 panel A (increased signal output) and a blue dot in panel C (decreased signal output). The shaded
402 areas represent the mean signal output from the Cys-less variant of EnvZ with a range of one

403 standard error of mean. These values are provided to aid in comparison. Error bars represent
404 standard deviation of the mean with a sample size of n ≥ 3.

405 Figure 3. Extent of sulfhydryl-reactivity for each single-Cys-containing EnvZ variant.
406 EPB30/pRD400 cells were grown under the low- (empty circles, 0% sucrose) or high-osmolarity
407 (filled circles, 15% sucrose) regimes and subjected to 250 μM molecular iodine for 10 minutes
408 when their OD_{600nm} reached approximately 0.25. As shown in Figure S5, this allowed us to
409 determine the dimer/monomer ratio represented on the Y-axis. Three distinct regions, denoted I, II
410 and III were observed and are described in the text. Error bars represent the standard error of the
411 mean with a sample size of n ≥ 3.

412

413 Figure 4. Aromatic tuning and signal output from EnvZ. (A) When aromatic tuning was performed
414 in EnvZ, a Trp-Leu-Phe triplet (red) was repositioned within the C-terminal region of TM2. (B)
415 Helix displacements, (C) tilt distributions and (D) azimuthal rotational distributions of the
416 aromatically tuned EnvZ TM2 helices. Histograms are shown for all time points of all membranes
417 of each ensemble. Aromatically tuned mutants have been classified based on their signal output into
418 five categories: highly kinase biased (WLF-1; pink), moderately kinase biased (WLF-5, WLF-4,
419 WLF-3; red), balanced (wild-type; black), moderately phosphatase biased (WLF-2, WLF+1, dark
420 blue) and highly phosphatase biased (WLF+2, light blue).

421

422 **References**

423

424 *1 Delcour, A. H. Solute uptake through general porins. Frontiers in bioscience : a journal and*
425 *virtual library **8**, d1055-1071, (2003).*
426 *2 Nikaido, H. Molecular basis of bacterial outer membrane permeability revisited.*
427 *Microbiology and molecular biology reviews : MMBR **67**, 593-656, (2003).*
428 *3 Elliott, E. et al. In vivo development of ertapenem resistance in a patient with pneumonia*
429 *caused by Klebsiella pneumoniae with an extended-spectrum beta-lactamase. Clinical*

430 *infectious diseases : an official publication of the Infectious Diseases Society of America **42**,*
431 *e95-98, (2006).*
432 4 *Hernandez-Alles, S. et al. Relationship between outer membrane alterations and*
433 *susceptibility to antimicrobial agents in isogenic strains of Klebsiella pneumoniae. The*
434 *Journal of antimicrobial chemotherapy **46**, 273-277, (2000).*
435 5 *Jacoby, G. A., Mills, D. M. & Chow, N. Role of beta-lactamases and porins in resistance to*
436 *ertapenem and other beta-lactams in Klebsiella pneumoniae. Antimicrob. Agents*
437 *Chemother. **48**, 3203-3206, (2004).*
438 6 *Kaczmarek, F. M., Dib-Hajj, F., Shang, W. & Gootz, T. D. High-level carbapenem*
439 *resistance in a Klebsiella pneumoniae clinical isolate is due to the combination of bla(ACT-*
440 *1) beta-lactamase production, porin OmpK35/36 insertional inactivation, and down-*
441 *regulation of the phosphate transport porin phoe. Antimicrob. Agents Chemother. **50**, 3396-*
442 *3406, (2006).*
443 7 *Loli, A. et al. Sources of diversity of carbapenem resistance levels in Klebsiella pneumoniae*
444 *carrying blaVIM-1. The Journal of antimicrobial chemotherapy **58**, 669-672, (2006).*
445 8 *Martinez-Martinez, L. et al. Activities of imipenem and cephalosporins against clonally*
446 *related strains of Escherichia coli hyperproducing chromosomal beta-lactamase and*
447 *showing altered porin profiles. Antimicrob. Agents Chemother. **44**, 2534-2536, (2000).*
448 9 *Mena, A. et al. Characterization of a large outbreak by CTX-M-1-producing Klebsiella*
449 *pneumoniae and mechanisms leading to in vivo carbapenem resistance development. J Clin*
450 *Microbiol **44**, 2831-2837, (2006).*
451 10 *Egger, L. A. & Inouye, M. Purification and characterization of the periplasmic domain of*
452 *EnvZ osmosensor in Escherichia coli. Biochem. Biophys. Res. Commun. **231**, 68-72, (1997).*
453 11 *Forst, S. A. & Roberts, D. L. Signal transduction by the EnvZ-OmpR phosphotransfer*
454 *system in bacteria. Research in microbiology **145**, 363-373, (1994).*
455 12 *Mizuno, T. His-Asp phosphotransfer signal transduction. J Biochem **123**, 555-563, (1998).*
456 13 *Hoch, J. A. & Silhavy, T. J. (American Society of Microbiology Press, Washington, DC,*
457 *USA, 1995).*
458 14 *Gerken, H., Charlson, E. S., Cicirelli, E. M., Kenney, L. J. & Misra, R. MzrA: a novel*
459 *modulator of the EnvZ/OmpR two-component regulon. Mol Microbiol **72**, 1408-1422,*
460 *(2009).*
461 15 *Gerken, H. & Misra, R. MzrA-EnvZ interactions in the periplasm influence the EnvZ/OmpR*
462 *two-component regulon. J Bacteriol **192**, 6271-6278, (2010).*
463 16 *Forst, S. A., Delgado, J. & Inouye, M. DNA-binding properties of the transcription activator*
464 *(OmpR) for the upstream sequences of ompF in Escherichia coli are altered by envZ*
465 *mutations and medium osmolarity. J Bacteriol **171**, 2949-2955, (1989).*
466 17 *Lan, C. Y. & Igo, M. M. Differential expression of the OmpF and OmpC porin proteins in*
467 *Escherichia coli K-12 depends upon the level of active OmpR. J Bacteriol **180**, 171-174,*
468 *(1998).*
469 18 *Russo, F. D. & Silhavy, T. J. EnvZ controls the concentration of phosphorylated OmpR to*
470 *mediate osmoregulation of the porin genes. J Mol Biol **222**, 567-580, (1991).*
471 19 *Adler, M., Anjum, M., Andersson, D. I. & Sandegren, L. Combinations of mutations in envZ,*
472 *ftsI, mrdA, acrB and acrR can cause high-level carbapenem resistance in Escherichia coli.*
473 *The Journal of antimicrobial chemotherapy **71**, 1188-1198, (2016).*
474 20 *Gushchin, I. et al. Mechanism of transmembrane signaling by sensor histidine kinases.*
475 *Science, (2017).*
476 21 *Unnerstale, S., Maler, L. & Draheim, R. R. Structural characterization of AS1-membrane*
477 *interactions from a subset of HAMP domains. Biochim Biophys Acta **1808**, 2403-2412,*
478 *(2011).*

479 22 *Hulko, M. et al. The HAMP domain structure implies helix rotation in transmembrane*
480 *signaling. Cell **126**, 929-940, (2006).*
481 23 *Zhou, Q., Ames, P. & Parkinson, J. S. Mutational analyses of HAMP helices suggest a*
482 *dynamic bundle model of input-output signalling in chemoreceptors. Mol Microbiol **73**,*
483 *801-814, (2009).*
484 24 *Falke, J. J. & Hazelbauer, G. L. Transmembrane signaling in bacterial chemoreceptors.*
485 *Trends in biochemical sciences **26**, 257-265, (2001).*
486 25 *Hazelbauer, G. L., Falke, J. J. & Parkinson, J. S. Bacterial chemoreceptors: high-*
487 *performance signaling in networked arrays. Trends in biochemical sciences **33**, 9-19,*
488 *(2008).*
489 26 *Parkinson, J. S., Hazelbauer, G. L. & Falke, J. J. Signaling and sensory adaptation in*
490 *Escherichia coli chemoreceptors: 2015 update. Trends in microbiology **23**, 257-266, (2015).*
491 27 *Hwang, E. et al. Crystal structure of the EnvZ periplasmic domain with CHAPS. FEBS Lett*
492 ***591**, 1419-1428, (2017).*
493 28 *Upadhyay, A. A., Fleetwood, A. D., Adebali, O., Finn, R. D. & Zhulin, I. B. Cache Domains*
494 *That are Homologous to, but Different from PAS Domains Comprise the Largest*
495 *Superfamily of Extracellular Sensors in Prokaryotes. PLoS computational biology **12**,*
496 *e1004862, (2016).*
497 29 *Heininger, A., Yusuf, R., Lawrence, R. & Draheim, R. R. Identification of transmembrane*
498 *helix 1 (TM1) surfaces important for EnvZ dimerisation and signal output. Biochim.*
499 *Biophys. Acta **1858**, 1868-1875, (2016).*
500 30 *Hessa, T. et al. Molecular code for transmembrane-helix recognition by the Sec61*
501 *translocon. Nature **450**, 1026-1030, (2007).*
502 31 *Krogh, A., Larsson, B., von Heijne, G. & Sonnhammer, E. L. Predicting transmembrane*
503 *protein topology with a hidden Markov model: application to complete genomes. J Mol Biol*
504 ***305**, 567-580, (2001).*
505 32 *Adase, C. A., Draheim, R. R. & Manson, M. D. The residue composition of the aromatic*
506 *anchor of the second transmembrane helix determines the signaling properties of the*
507 *aspartate/maltose chemoreceptor Tar of Escherichia coli. Biochemistry **51**, 1925-1932,*
508 *(2012).*
509 33 *Adase, C. A., Draheim, R. R., Rueda, G., Desai, R. & Manson, M. D. Residues at the*
510 *cytoplasmic end of transmembrane helix 2 determine the signal output of the TarEc*
511 *chemoreceptor. Biochemistry **52**, 2729-2738, (2013).*
512 34 *Wright, G. A., Crowder, R. L., Draheim, R. R. & Manson, M. D. Mutational analysis of the*
513 *transmembrane helix 2-HAMP domain connection in the Escherichia coli aspartate*
514 *chemoreceptor tar. J Bacteriol **193**, 82-90, (2011).*
515 35 *Bass, R. B., Butler, S. L., Chervitz, S. A., Gloor, S. L. & Falke, J. J. Use of site-directed*
516 *cysteine and disulfide chemistry to probe protein structure and dynamics: applications to*
517 *soluble and transmembrane receptors of bacterial chemotaxis. Methods in enzymology **423**,*
518 *25-51, (2007).*
519 36 *Draheim, R. R., Bormans, A. F., Lai, R. Z. & Manson, M. D. Tuning a bacterial*
520 *chemoreceptor with protein-membrane interactions. Biochemistry **45**, 14655-14664, (2006).*
521 37 *Botelho, S. C., Enquist, K., von Heijne, G. & Draheim, R. R. Differential repositioning of*
522 *the second transmembrane helices from E. coli Tar and EnvZ upon moving the flanking*
523 *aromatic residues. Biochim Biophys Acta **1848**, 615-621, (2015).*
524 38 *Hall, B. A., Armitage, J. P. & Sansom, M. S. Transmembrane helix dynamics of bacterial*
525 *chemoreceptors supports a piston model of signalling. PLoS computational biology **7**,*
526 *e1002204, (2011).*
527 39 *Mise, T. Structural Analysis of the Ligand-Binding Domain of the Aspartate Receptor Tar*
528 *from Escherichia coli. Biochemistry **55**, 3708-3713, (2016).*

529 40 *Norholm, M. H., von Heijne, G. & Draheim, R. R. Forcing the Issue: Aromatic Tuning*
530 *Facilitates Stimulus-Independent Modulation of a Two-Component Signaling Circuit. ACS*
531 *Synth Biol **4**, 474-481, (2015).*
532 41 *Batchelor, E. & Goulian, M. Robustness and the cycle of phosphorylation and*
533 *dephosphorylation in a two-component regulatory system. Proc Natl Acad Sci U S A **100**,*
534 *691-696, (2003).*
535 42 *Miyashiro, T. & Goulian, M. High stimulus unmasks positive feedback in an autoregulated*
536 *bacterial signaling circuit. Proc Natl Acad Sci U S A **105**, 17457-17462, (2008).*
537 43 *Siryaporn, A. & Goulian, M. Cross-talk suppression between the CpxA-CpxR and EnvZ-*
538 *OmpR two-component systems in E. coli. Mol Microbiol **70**, 494-506, (2008).*
539 44 *Chervitz, S. A. & Falke, J. J. Molecular mechanism of transmembrane signaling by the*
540 *aspartate receptor: a model. Proc Natl Acad Sci U S A **93**, 2545-2550, (1996).*
541 45 *Falke, J. J. Piston versus Scissors: Chemotaxis Receptors versus Sensor His-Kinase*
542 *Receptors in Two-Component Signaling Pathways. Structure **22**, 1219-1220, (2014).*
543 46 *Molnar, K. S. et al. Cys-Scanning Disulfide Crosslinking and Bayesian Modeling Probe the*
544 *Transmembrane Signaling Mechanism of the Histidine Kinase, PhoQ. Structure **22**, 1239-*
545 *1251, (2014).*
546 47 *Cheung, J., Bingman, C. A., Reyngold, M., Hendrickson, W. A. & Waldburger, C. D. Crystal*
547 *structure of a functional dimer of the PhoQ sensor domain. J Biol Chem **283**, 13762-13770,*
548 *(2008).*
549 48 *Inouye, M. Signaling by transmembrane proteins shifts gears. Cell **126**, 829-831, (2006).*
550 49 *Yusuf, R. & Draheim, R. R. Employing aromatic tuning to modulate output from two-*
551 *component signaling circuits. J Biol Eng **9**, 7, (2015).*
552 50 *Casadaban, M. J. & Cohen, S. N. Analysis of gene control signals by DNA fusion and*
553 *cloning in Escherichia coli. J Mol Biol **138**, 179-207, (1980).*
554 51 *Guyer, M. S., Reed, R. R., Steitz, J. A. & Low, K. B. Identification of a sex-factor-affinity site*
555 *in E. coli as gamma delta. Cold Spring Harb Symp Quant Biol **45 Pt 1**, 135-140, (1981).*
556 52 *Batchelor, E., Silhavy, T. J. & Goulian, M. Continuous control in bacterial regulatory*
557 *circuits. J Bacteriol **186**, 7618-7625, (2004).*
558 53 *Hsing, W. & Silhavy, T. J. Function of conserved histidine-243 in phosphatase activity of*
559 *EnvZ, the sensor for porin osmoregulation in Escherichia coli. J Bacteriol **179**, 3729-3735,*
560 *(1997).*
561 54 *Cantwell, B. J. et al. CheZ phosphatase localizes to chemoreceptor patches via CheA-short.*
562 *J Bacteriol **185**, 2354-2361, (2003).*
563 55 *Southern, J. A., Young, D. F., Heaney, F., Baumgartner, W. K. & Randall, R. E.*
564 *Identification of an epitope on the P and V proteins of simian virus 5 that distinguishes*
565 *between two isolates with different biological characteristics. The Journal of general*
566 *virology **72 (Pt 7)**, 1551-1557, (1991).*
567 56 *Lai, R. Z., Bormans, A. F., Draheim, R. R., Wright, G. A. & Manson, M. D. The region*
568 *preceding the C-terminal NWETF pentapeptide modulates baseline activity and aspartate*
569 *inhibition of Escherichia coli Tar. Biochemistry **47**, 13287-13295, (2008).*
570 57 *Lehning, C. E., Heidelberger, J. B., Reinhard, J., Norholm, M. H. & Draheim, R. R. A*
571 *Modular High-Throughput In Vivo Screening Platform Based on Chimeric Bacterial*
572 *Receptors. ACS Synth Biol, (2017).*
573 58 *Miller, J. H. A Short Course in Bacterial Genetics: A Laboratory Manual and Handbook for*
574 *Escherichia coli and Related Bacteria. (Cold Spring Harbor Laboratory Press, 1992).*
575 59 *Ausubel, F. M. et al. Current Protocols in Molecular Biology. (Wiley, 1998).*
576 60 *Schneider, C. A., Rasband, W. S. & Eliceiri, K. W. NIH Image to ImageJ: 25 years of image*
577 *analysis. Nat Methods **9**, 671-675, (2012).*

578 *61* *Van Der Spoel, D. et al. GROMACS: fast, flexible, and free. Journal of computational*
579 *chemistry* ***26****, 1701-1718, (2005).*
580
581

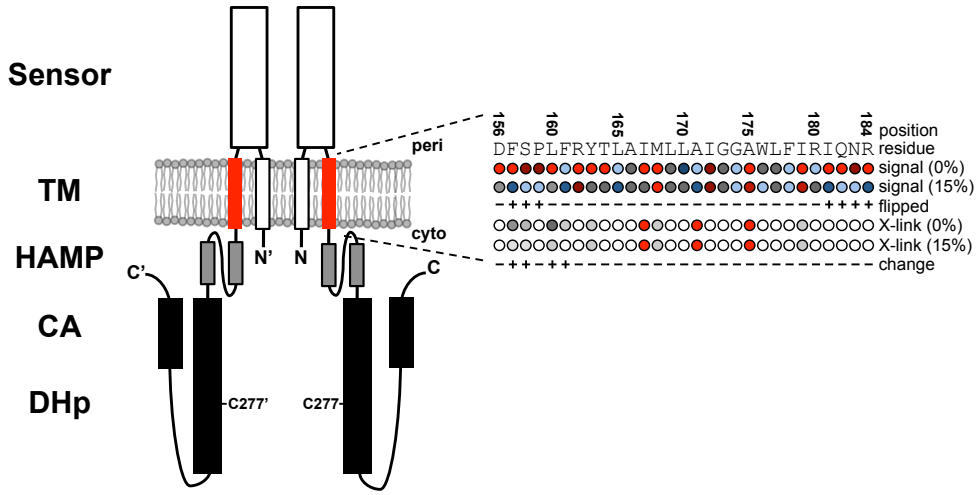
Sensor
TM
HAMP
CA
DHp
peri
cyto
N'
N
C'
C
C277'
C277
156
160
165
170
175
180
184
position
DFSPLFRYTLAIMLLAIGGAWLFIRIQNR
residue
signal (0%)
signal (15%)
flipped
X-link (0%)
X-link (15%)
change

Figure 1.

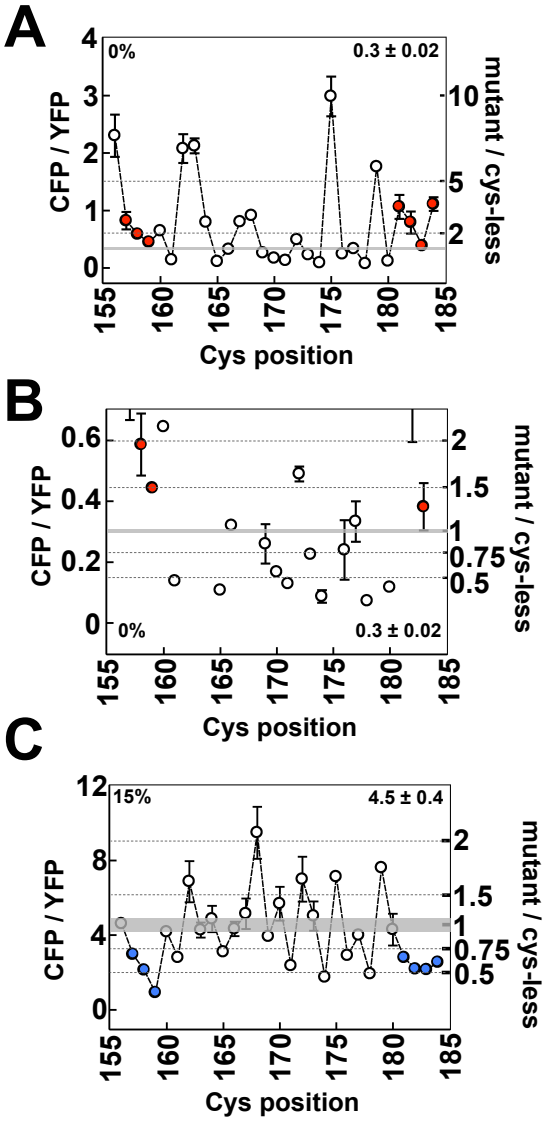
A
0%
0.3 ± 0.02
CFP / YFP
mutant / cys-less
Cys position
B
0%
0.3 ± 0.02
CFP / YFP
mutant / cys-less
Cys position
C
15%
4.5 ± 0.4
CFP / YFP
mutant / cys-less
Cys position

Figure 2.

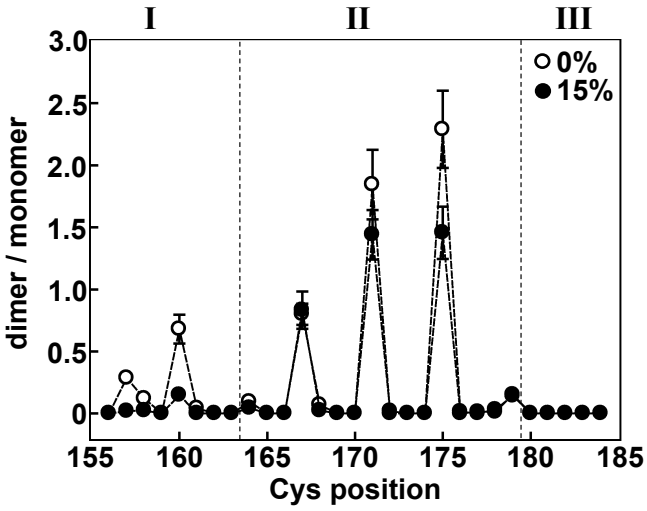
I
II
III
0%
15%
dimer / monomer
3.0
2.5
2.0
1.5
1.0
0.5
0
155
160
165
170
175
180
185
Cys position

Figure 3.

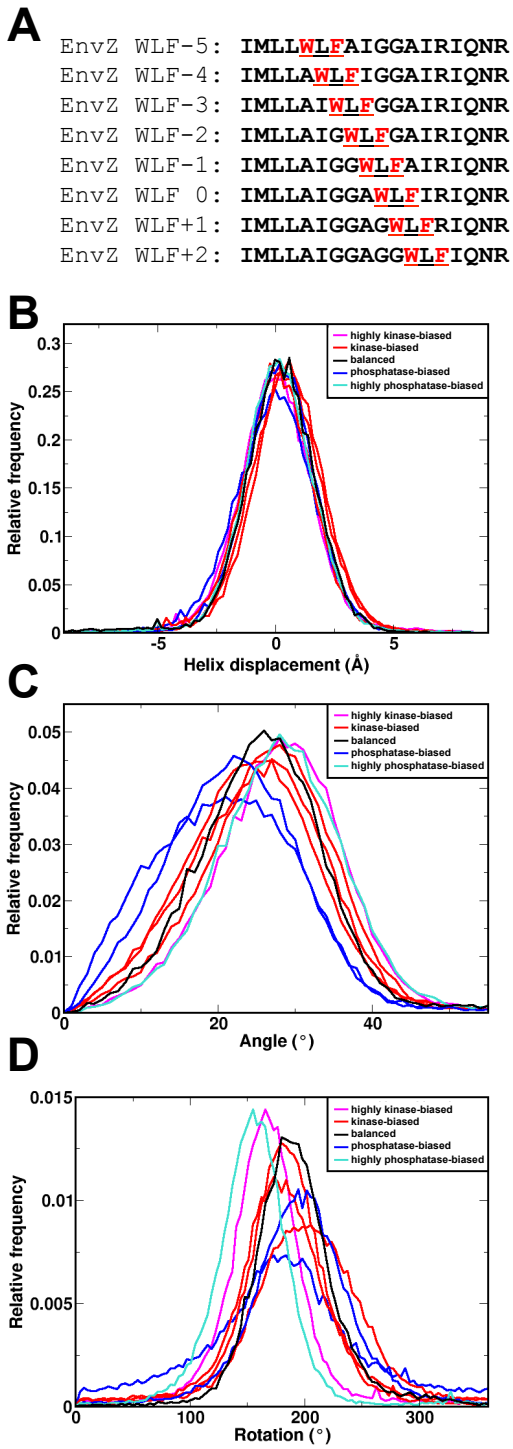
A
EnvZ WLF-5: IMLLWLFAIGGAIRIQNR
EnvZ WLF-4: IMLLAWLFIGGAIRIQNR
EnvZ WLF-3: IMLLAIWLFGGAIRIQNR
EnvZ WLF-2: IMLLAIGWLFGAIRIQNR
EnvZ WLF-1: IMLLAIGGWLFAIRIQNR
EnvZ WLF 0: IMLLAIGGAWLFIRIQNR
EnvZ WLF+1: IMLLAIGGAGWLFRIQNR
EnvZ WLF+2: IMLLAIGGAGGWLFIQNR
B
highly kinase-biased
kinase-biased
balanced
phosphatase-biased
highly phosphatase-biased
Relative frequency
Helix displacement (Å)
C
Angle (°)
D
Rotation (°)

Figure 4.